J|A|C|S
ARTICLES

Published on Web 12/07/2009

Size-Dependent Multiple Twinning in Nanocrystal Superlattices

Sara M. Rupich,[†] Elena V. Shevchenko,[‡] Maryna I. Bodnarchuk,[†] Byeongdu Lee,[§] and Dmitri V. Talapin*[,†,‡]

Department of Chemistry, The University of Chicago, Chicago, Illinois 60637, and Center for Nanoscale Materials and Advanced Photon Source, Argonne National Laboratory, Argonne, Illinois 60439

Received September 3, 2009; E-mail: dvtalapin@uchicago.edu

Abstract: We report a size-dependent change in the morphology of superlattices self-assembled from monodisperse colloidal PbS nanocrystals. Superlattices of large (>7 nm) PbS nanocrystals showed a strong tendency to form multiply twinned face-centered cubic superlattices with decahedral and icosahedral symmetry, exhibiting crystallographically forbidden five-fold symmetry elements. On the other hand, superlattices of small (<4 nm) PbS nanocrystals exhibited no twinning. To explain such a dramatic difference in the twinning probability, we showed that twinning energy in a nanocrystal superlattice is strongly size-dependent. In addition, the interparticle potentials acting during the self-assembly process are "softer" in the case of larger PbS nanocrystals, thus favoring the formation of multiply twinned superlattices. Our work introduces a new class of materials exhibiting multiple twinning, while offering flexibility in designing interparticle potentials.

1. Introduction

Monodisperse colloidal nanoparticles can self-assemble into ordered arrays (superlattices).[1,2] Previous studies have illustrated the ability to grow superlattices from metallic,[2–4] semiconductor,[1] and magnetic nanocrystals[5] as well as binary mixtures.[6–8] The discovery of very rich phase diagrams inherent to binary nanoparticle superlattices[9] opened up exciting opportunities for making complex ordered structures built from several functional components. A deep understanding of the fundamental principles that govern self-assembly of nanoparticles into single- and multicomponent superlattices is crucially important for the development of nanocrystal-based devices, such as LEDs,[10,11] solar cells,[12] photodetectors,[13] and thermoelectric heat-to-electricity converters.[14] From a different perspective, many features present in ordinary crystals (translational symmetry, faceting, polytypism, defects, etc.) have been observed in nanocrystal superlattices, suggesting that their assembly follows the same fundamental principles driving the crystallization of atomic and molecular solids. In contrast to individual atoms and molecules, which are very difficult to image in real space, nanoparticles and their superstructures can be studied in great detail using conventional electron microscopy. In this regard, the investigation of nanoparticle self-assembly can help in studying general aspects of crystallization and surface structure using powerful real-space imaging techniques.[15]

In this work, we look at twinning in nanocrystal superlattices and show how interparticle interactions affect the energy of twin plane formation and determine the equilibrium shape of nanocrystal superlattices. According to the International Union of Crystallography, twinning is the oriented association of two or more individuals in the same crystalline phase, which are related by a geometrical operation, termed "twin operation" (typically a simple mirror reflection of the lattice).[16] This operation cannot belong to the symmetry of the crystal; otherwise, it would produce a parallel growth instead of a twin plane. In the case of a face-centered cubic (fcc) lattice, formation of a twin plane

[†] The University of Chicago.
[‡] Center for Nanoscale Materials, ANL.
[§] Advanced Photon Source, ANL.

(1) Murray, C. B.; Kagan, C. R.; Bawendi, M. G. *Annu. Rev. Mater. Sci.* **2000**, *30*, 545–610.
(2) Whetten, R. L.; Shafigullin, M. N.; Khoury, J. T.; Schaaff, T. G.; Vezmar, I.; Alvarez, M. M.; Wilkinson, A. *Acc. Chem. Res.* **1999**, *32*, 397–406.
(3) Zheng, N.; Fan, J.; Stucky, G. D. *J. Am. Chem. Soc.* **2006**, *128*, 6550–6551.
(4) Korgel, B. A.; Fullam, S.; Connolly, S.; Fitzmaurice, D. *J. Phys. Chem. B* **1998**, *102*, 8379–8388.
(5) Murray, C. B.; Sun, S. H.; Doyle, H.; Betley, T. *MRS Bull.* **2001**, *26*, 985–991.
(6) Kiely, C. J.; Fink, J.; Brust, M.; Bethel, D.; Schiffrin, D. J. *Nature* **1998**, *396*, 444–446.
(7) Overgaag, K.; Evers, W.; de Nijs, B.; Koole, R.; Meeldijk, J.; Vanmaekelbergh, D. *J. Am. Chem. Soc.* **2008**, *130*, 7833–7835.
(8) Saunders, A. E.; Korgel, B. A. *ChemPhysChem* **2005**, *6*, 61–65.
(9) Shevchenko, E. V.; Talapin, D. V.; Murray, C. B.; O'Brien, S. *J. Am. Chem. Soc.* **2006**, *128*, 3620–3637.
(10) Coe, S.; Woo, W. K.; Bawendi, M.; Bulovic, V. *Nature* **2002**, *420*, 800–803.
(11) Colvin, V. L.; Schlamp, M. C.; Alivisatos, A. P. *Nature* **1994**, *370*, 354–357.
(12) Huynh, W. U.; Dittmer, J. J.; Alivisatos, A. P. *Science* **2002**, *295*, 2425–2427.
(13) Konstantatos, G.; Howard, I.; Fischer, A.; Hoogland, S.; Clifford, J.; Klem, E.; Levina, L.; Sargent, E. H. *Nature* **2006**, *442*, 180–183.
(14) Poudel, B.; Hao, Q.; Ma, Y.; Lan, Y.; Minnich, A.; Yu, B.; Yan, X.; Wang, D.; Muto, A.; Vashaee, D.; Chen, X.; Liu, J.; Dresselhaus, M. S.; Chen, G.; Ren, Z. *Science* **2008**, *320*, 634–638.
(15) Wang, Z. L. *Adv. Mater.* **1998**, *10*, 13–30.
(16) International Union of Crystallography: http://www.crystallography.fr/mathcryst/twins.htm.

occurs when the fcc packing sequence of the (111) planes (ABCABC...) is disrupted by the reflection of the planes across the twin boundary (ABCBAC...). Twinning has been observed in many fcc metals (Au, Ag, Pt, Pd)[17−21] along with Si[22,23] and diamond.[24,25] It should not be considered as simply a crystal imperfection, as it plays an important role in the thermodynamics and kinetics of crystal growth. For example, the formation of twin planes determines the equilibrium shapes of small noble metal particles[20,26−31] and is often responsible for the anisotropic growth of plate-like crystals.[32−35] Probably the most amazing manifestation of the twinning phenomenon is the formation of multiply twinned (MT) particles with decahedral and icosahedral shapes, where multiple twin planes form and intersect in a characteristic manner, resulting in crystals possessing "forbidden" five-fold symmetry elements.

Taking into account similarities between the growth of ordinary crystals and the self-assembly of nanocrystal superlattices, it would be reasonable to expect that twinning can occur in superlattice formation. Indeed, examples of twinned structures can be found in previously published scanning electron microscopy images of nanoparticle superlattices.[15,36−38] At the same time, to the best of our knowledge, the energetics and driving forces behind twinning in nanoparticle superlattices have never been studied or discussed.

2. Experimental Section

Synthesis of PbS Nanocrystals. In a typical synthesis, 0.758 g of lead acetate trihydrate was dissolved in 20 mL of oleic acid in a 100 mL three-neck flask and degassed by heating to 110 °C under vacuum for 1 h. The solution was heated to 145 °C under a nitrogen atmosphere, and 0.21 mL of hexamethyldisilathiane [$(TMS)_2S$] dissolved in 10 mL of dried 1-octadecene was injected into the reaction mixture. The heat source was immediately removed, and the reaction continued for 3.5 min before quenching. The nanocrystals were isolated by rinsing with hexane and precipitation with ethanol followed by centrifugation. The washing was repeated once, and the nanocrystals were stored in chloroform. The size of the nanocrystals was controlled by varying the reaction parameters. Larger nanocrystals were synthesized by decreasing the volume of octadecene used to carry the sulfur precursor, while smaller nanocrystals were synthesized by decreasing the volume of oleic acid to a minimum of 1.25 mL and adding octadecene until a total volume of 20 mL was reached.

Growth of the Superlattices of PbS Nanocrystals. The crystallization of PbS nanocrystals was carried out through a two-layer phase diffusion technique in vertically positioned glass test tubes. We grew three-dimensional superlattices of PbS nanocrystals by slowly destabilizing the colloidal solutions.[40,41] In a typical experiment, we filled a 0.8 cm inner diameter glass tube with 1.2 mL of a colloidal solution of PbS nanocrystals in toluene (~1 mg/mL). A layer of ethanol was carefully added above the colloidal solution of nanocrystals, as shown in Figure 1c. The tube was sealed and left in the dark for approximately 1 week. During this time, the nanocrystal superlattices nucleated and grew on the walls of the tube and on the thin silicon substrate positioned vertically in the tube (Figure 1c). After completion of the experiment, the solvent was carefully removed, the substrate was taken out of the tube and rinsed with acetone, and the superlattices were investigated by optical microscopy and SEM.

Characterization. Optical microscopy, SEM, high-resolution SEM, and small-angle X-ray scattering were used to characterize the superlattices. Optical images were taken on an Olympus BX51 microscope. SEM images were obtained using either an FEI Nova NanoSEM 200 operated between 3.0 and 10.0 kV or a JEOL JSM-5800LV microscope operated at 5 kV. For all microscopy, imaging was carried out on the silicon wafer, and for HRSEM the samples were rinsed with acetone to remove excessive organic ligands. Small-angle X-ray scattering (SAXS) measurements were performed at Argonne National Laboratory at the APS 12ID beamline with X-ray energy of 12 keV. The sample-to-detector distance was ~2 m. Dynamic light scattering and electrophoretic mobility measurements were carried out using a Zetasizer Nano-ZS (Malvern Instruments, UK). Colloidal solutions were transferred into a quartz cuvette, and the dip cell electrode assembly with Pd electrodes was used to apply an electric field to solution. Dilution was optimized for each sample to achieve >100 kcps count rate and the best signal-to-noise ratio.

3. Results and Discussion

We studied superlattices composed of PbS nanocrystals capped with oleic acid surface ligands. PbS nanocrystals are a convenient model system for colloidal crystallization because of the ability to easily achieve narrow nanocrystal size distributions, the possibility of precisely tuning the nanocrystal size from ~2 up to >10 nm,[39] and their stability under ambient conditions. Typical transmission electron microscopy images of monolayers of 3.1 and 8.0 nm diameter PbS nanocrystals are shown in Figure 1a and b, respectively.

Analysis of a large number (>50) of nanocrystal samples revealed a remarkable trend in the morphology of the self-assembled superlattices. Smaller (<4 nm) PbS nanocrystals typically self-assembled into well-faceted platelet-shaped superlattices (Figures 1d and 2a), whereas larger (>7 nm) nanocrystals formed superlattices with more complex shapes (Figure 1e). The most common shapes are illustrated in Figure 2c−f. Despite apparent "imperfect" shapes, the superlattices of larger PbS nanocrystals showed well-resolved small-angle X-ray

(17) Crampin, S.; Hampel, K.; Vvedensky, D. D.; Maclaren, J. M. *J. Mater. Res.* **1990**, *5*, 2107–2119.
(18) Dahmen, U.; Hetherington, C. J. D.; Radmilovic, V.; Johnson, E.; Xiao, S. Q.; Luo, C. P. *Microsc. Microanal.* **2002**, *8*, 247–256.
(19) Rosengaard, N. M.; Skriver, H. L. *Phys. Rev. B* **1993**, *47*, 12865–12873.
(20) Ino, S.; Ogawa, S. *J. Phys. Soc. Jpn.* **1967**, *22*, 1365–1374.
(21) Marks, L. D.; Smith, D. J. *J. Cryst. Growth* **1981**, *54*, 425–432.
(22) Iijima, S. *Jpn. J. Appl. Phys., Part 1* **1987**, *26*, 357–364.
(23) Iijima, S. *Jpn. J. Appl. Phys., Part 1* **1987**, *26*, 365–372.
(24) Mani, R. C.; Sunkara, M. K. *Diamond Relat. Mater.* **2003**, *12*, 324–329.
(25) Son, S. I.; Chung, S. J. *Z. Kristallogr.* **2004**, *219*, 494–505.
(26) Xia, Y.; Xiong, Y. J.; Lim, B.; Skrabalak, S. E. *Angew. Chem., Int. Ed.* **2009**, *48*, 60–103.
(27) Ino, S. *J. Phys. Soc. Jpn.* **1969**, *27*, 941–953.
(28) Hofmeister, H. *Cryst. Res. Technol.* **1998**, *33*, 3–25.
(29) Howie, A.; Marks, L. D. *Philos. Mag. A* **1984**, *49*, 95–109.
(30) Marks, L. D. *Philos. Mag. A* **1984**, *49*, 81–93.
(31) Maskay, A. L. *Acta Crystallogr.* **1962**, *15*, 916–918.
(32) Elechiguerra, J. L.; Reyes-Gasga, J.; Yacaman, M. J. *J. Mater. Chem.* **2006**, *16*, 3906–3919.
(33) Lofton, C.; Sigmund, W. *Adv. Funct. Mater.* **2005**, *15*, 1197–1208.
(34) Jagannathan, S.; Chen, S.; Mehta, R. V.; Jagannathan, R. *Phys. Rev. B* **1996**, *53*, 9–11.
(35) Bogels, G.; Meekes, H.; Bennema, P.; Bollen, D. *J. Phys. Chem. B* **1999**, *103*, 7577–7583.
(36) Bishop, K. J. M.; Wilmer, C. E.; Soh, S.; Grzybowski, B. A. *Small* **2009**, *5*, 1600–1630.
(37) Nagel, M.; Hickey, S. G.; Fromsdorf, A.; Kornowski, A.; Weller, H. *Z. Phys. Chem.: Int. J. Res. Phys. Chem. Chem. Phys.* **2007**, *221*, 427–437.
(38) Yao, H.; Kimura, K. *Mod. Res. Educ. Top. Microsc.* **2007**, 568–575.
(39) Hines, M. A.; Scholes, G. D. *Adv. Mater.* **2003**, *15*, 1844–1849.
(40) Talapin, D. V.; Shevchenko, E. V.; Kornowski, A.; Gaponik, N.; Haase, M.; Rogach, A. L.; Weller, H. *Adv. Mater.* **2001**, *13*, 1868–1871.
(41) Talapin, D. V.; Shevchenko, E. V.; Murray, C. B.; Kornowski, A.; Förster, S.; Weller, H. *J. Am. Chem. Soc.* **2004**, *126*, 12984–12988.

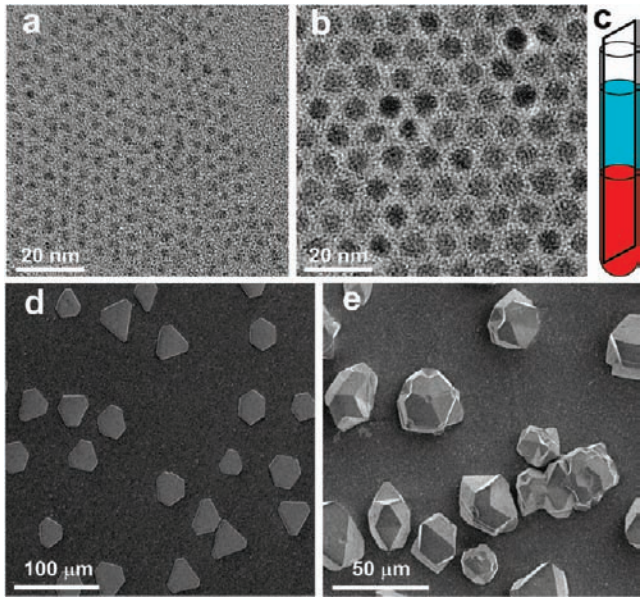

Figure 1. TEM images of (a) 3.1 and (b) 8.0 nm PbS nanocrystals. (c) A scheme illustrating the oversaturation technique used for growing superlattices: red, the colloidal solution of PbS nanocrystals in toluene; blue, the layer of ethanol. A silicon wafer was placed inside the tube as a substrate for growing superlattices. (d,e) Superlattices grown from 3.1 and 8 nm PbS nanocrystals, respectively. A significant difference is observed in the morphologies of the superlattices grown from 8 and 3.1 nm nanocrystals.

reflections, characteristic of long-range fcc ordering of the individual nanocrystals (Figure 3).

For single crystals with a perfect fcc lattice, the Wulff construction predicts a truncated octahedron that contains eight 111 facets and six 100 facets, known as the Wulff polyhedron; this shape minimizes the overall surface energy of the crystal.[29,32] Obviously, the morphologies that predominate in superlattices of 8 nm PbS nanocrystals are different from the Wulff polyhedron. A closer look revealed that the observed morphological complexity has its origin in the presence of twin planes along the (111) crystallographic direction. The intriguing observation is that the probability of twin formation in nanocrystal superlattices appears to be strongly size-dependent. In our experiments, superlattices of 3−4 nm PbS nanocrystals exhibited very few, if any, twin planes (Figures 1d and 2a), 5−6 nm nanocrystals formed superlattices that usually incorporated one or several parallel twin planes (e.g., Figure 2b) with the occasional more complex structure, whereas 7 nm and larger PbS nanocrystals regularly formed structures with multiple twin planes forming decahedral and icosahedral nanocrystal superlattices (Figure 2c−f), further referred to as "multiply twinned superlattices" (MT-SLs). The same qualitative trend has been observed for other nanocrystal materials (Au, CdSe), where an increase in the nanocrystal size increased the probability of formation of twin planes in close-packed nanocrystal assemblies.

The energetic contribution required for the formation of a twin plane is relatively small compared to other types of planar defects. For example, in bulk fcc metals, the energetic cost associated with the formation of a twin plane is approximately 2 orders of magnitude less than the energy of formation for the same area of crystal surface.[17,19,29] Somewhat counterintuitively, the incorporation of twin planes in the fcc lattice can lower the total energy of the entire crystal by reducing the area of high-energy surface facets while keeping the surface-to-volume ratio as small as possible. Indeed, the presence of twin planes in

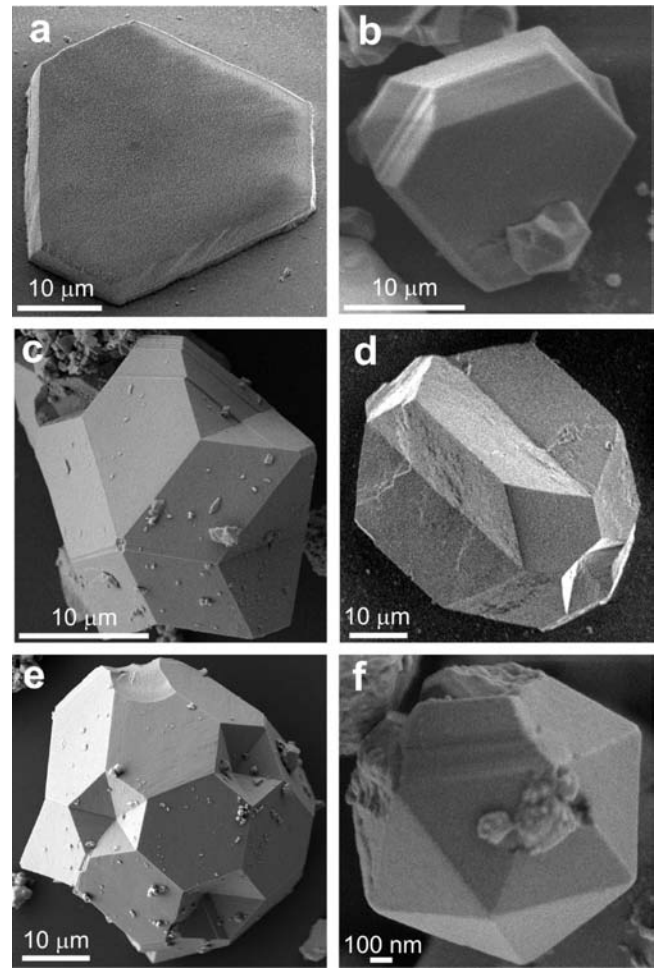

Figure 2. SEM images showing the characteristic morphologies for superlattices self-assembled from PbS nanocrystals of different sizes. (a) 3.1 nm PbS nanocrystals self-assembled in single-domain superstructures. (b) Superlattices of 5 nm PbS nanocrystals often incorporated a single twin plane or a few parallel twin planes. (c−f) 7 and 8 nm PbS nanocrystals formed multiply twinned superlattices with (c,d) decahedral and (e,f) icosahedral morphology.

superlattices shown in Figure 2c−f allows for the elimination of any facets except for the 111 facets known to be the lowest energy surfaces in fcc crystals.[32] Compared to any fcc crystals exhibiting only 111 facets (e.g., a tetrahedron or its various truncated forms), multitwinned structures possess smaller surface-to-volume ratios (Figure S1).[27] However, to make this possible, multiple twin planes need to orient themselves in one of two characteristic patterns. Five twin planes should arrange themselves symmetrically around an axis with D_{5h} point group symmetry, forming a decahedron or a star-shaped crystal (Figure 2c,d). Alternatively, 20 twin planes should orient themselves to intersect at a single point with icosahedral (I_h) point group symmetry, leading to crystals with icosahedral shapes (Figure 2e,f). Both of these multiply twinned structures have been extensively studied in atomic crystals.[26,29,32,33,42]

How Does Superlattice Twinning Energy Depend on the Nanocrystal Size? We calculated the specific additional energy associated with the twin plane formation in fcc nanocrystal superlattices, further referred to as "twinning energy". The individual nanocrystals were modeled as interacting spheres

(42) Gryaznov, V. G.; Heydenreich, J.; Kaprelov, A. M.; Nepijko, S. A.; Romanov, A. E.; Urban, J. *Cryst. Res. Technol.* **1999**, *34*, 1091–1119.

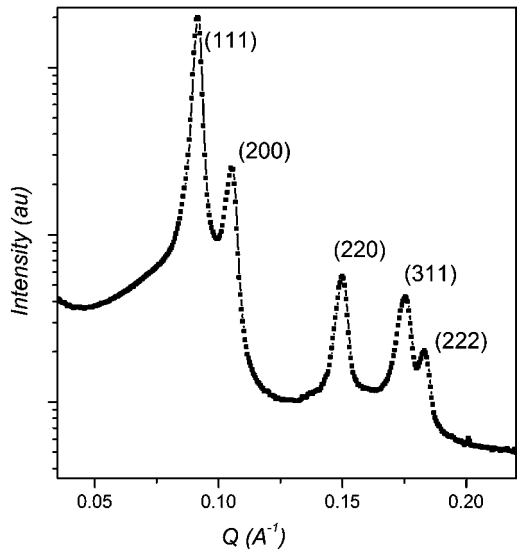

Figure 3. Small-angle X-ray diffraction measured from superlattices of the 7 nm PbS nanocrystals shown in Figure 2c,e. The small-angle reflections can be assigned to fcc packing of nanocrystals.

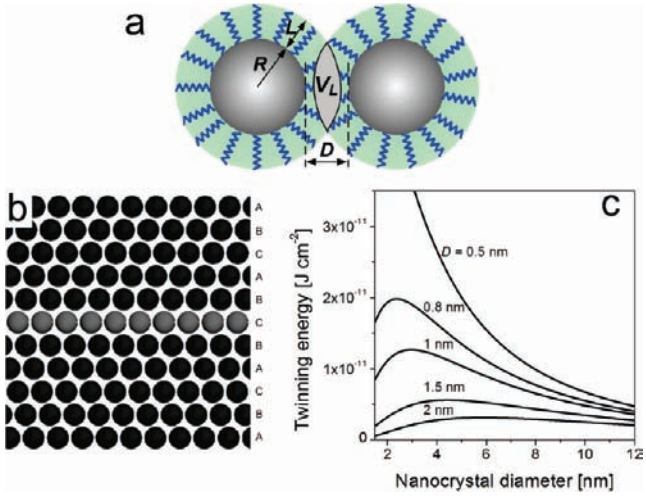

Figure 4. (a) Schematic of two interacting nanocrystals with radii of inorganic cores R and the effective thickness of the organic ligand shell L. If the separation between inorganic cores (D) is less than $2L$, the ligand shells will partially overlap with the overlap volume (V_L). (b) Schematic of a twin plane (highlighted in gray) in a fcc lattice viewed along the (110) projection. The sequence of the 111 planes undergoes reflection across the twin plane. (c) Twinning energy for fcc nanocrystal superlattices calculated for different interparticle separations (D) as a function of nanocrystal diameter. See text for details.

packed into a fcc lattice with interparticle interactions described by two-body pair potentials (Figure 4a). To calculate the twinning energy, we used a modified broken-bond method.[43] The additional energy required to form a twin plane with Miller indices h, k, and l can be obtained by comparing the total energy of pairwise interactions between individual particles in a perfect fcc superlattice to those in a superlattice incorporating a twin plane. The interparticle distances can be determined from the coordination spheres extending around a central nanocrystal, where the sphere radius is given by $r = a\sqrt{(h^2 + k^2 + l^2)}$, where a is the lattice parameter. In a perfect fcc lattice, each particle has 12 nearest neighbors with a center-to-center distance of $a/\sqrt{2}$, 6 second nearest neighbors at a, 24 third nearest neighbors at $a\sqrt{(3/2)}$, etc. (Table S1).[44] The presence of a twin plane leaves the nearest and second nearest neighbors untouched[19] while altering the location and number of third and further nearest neighbors (Figure 4b). Rather than having 24 third nearest neighbors, the nanocrystals located next to a twin plane have 21 third nearest neighbors unaffected by the structural modification, 1 neighbor located between the second and third coordination spheres, and 6 neighbors located between the third and fourth coordination spheres (Table S1 and Figure S2). The interparticle distances for particles located within the first six coordination spheres are given in Table S1.

To obtain the twinning energy, we need to know the dependence of the pair potentials on both the particle size and the interparticle distance. Electrophoretic mobility measurements revealed charge neutrality of PbS nanocrystals in toluene under our experimental conditions (Figure S3); therefore, the attractive part of the interparticle potential should be dominated by van der Waals (vdW) forces between both inorganic cores and ligand molecules. The vdW forces between the inorganic cores can be adequately described by eq 1:[4,45]

$$U_{\mathrm{vdW}}^{\mathrm{PbS-PbS}} = -\frac{A}{12}\left\{\frac{R}{D(1 + D/4R)} + \frac{1}{1 + D/R + D^2/4R^2} + 2\ln\left(\frac{D(1 + D/4R)}{R[1 + D/R + D^2/4R^2]}\right)\right\} \quad (1)$$

where A is the solvent-retarded Hamaker constant, R is the particle radius excluding the ligand shell, and D is the interparticle gap (for the nearest neighbors, D is maintained by surface ligands and is approximately 1 nm). The Hamaker constant for the system PbS/toluene/PbS can be estimated as ~0.3 eV.[46−48] It is much more difficult to accurately quantify the strength of the short-range vdW interactions between organic ligands, which can be either attractive or repulsive, depending on the nature of the solvent.[49] In addition, the short-range repulsion between nanocrystals has both elastic and steric components.[9,50] As a result, the interaction energy between nearest neighbors in nanocrystal superlattices should include multiple competing terms. Some of these issues will be discussed below. Fortunately, nearest neighbor interactions do not contribute to the twinning energy because no changes occur in the first coordination sphere. Therefore, the only force that matters in determining the twinning energy is described by the long-range part of the interparticle potential given in eq 1.

Figure 4c shows how the twinning energy per unit area (γ_t) depends on the nanocrystal size for different gaps between nanocrystals. As one can see, γ_t drops significantly with increasing nanocrystal size. This trend is much stronger for small interparticle gaps corresponding to short surface ligands but holds true up to $D \approx 1.5$ nm. Generally, the Hamaker constant A in eq 1 should be distance dependent due to the retardation

(43) Mackenzie, J. K.; Moore, A. J. W.; Nicholas, J. F. *J. Phys. Chem. Solids* **1962**, *23*, 185–196.
(44) Starostenkov, M. D. *Izv. Vyssh. Uchebn. Zaved., Fiz.* **1992**, *7*, 11–15.
(45) Ohara, P. C.; Leff, D. V.; Heath, J. R.; Gelbart, W. M. *Phys. Rev. Lett.* **1995**, *75*, 3466.
(46) Bergstrom, L. *Adv. Colloid Interface Sci.* **1997**, *70*, 125–169.
(47) Dong, K. J.; Yang, R. Y.; Zou, R. P.; Yu, A. B. *Phys. Rev. Lett.* **2006**, *96*, 145505.
(48) Saunders, B. R.; Turner, M. L. *Adv. Colloid Interface Sci.* **2008**, *138*, 1–23.
(49) Schapotschnikow, P.; Pool, R.; Vlugt, T. J. H. *Nano Lett.* **2008**, *8*, 2930–2934.
(50) Talapin, D. V.; Shevchenko, E. V.; Murray, C. B.; Titov, A. V.; Kral, P. *Nano Lett.* **2007**, *7*, 1213–1219.

effect. For example, accurate calculations based on the Dzyaloshinskii−Lifshitz−Pitaevskii theory predict that the Hamaker constant for two gold plates interacting through water should drop by ~50% at a separation distance of 30 nm.[36] Retardation should not play a significant role in the interparticle potential in superlattices composed of small nanocrystals. For example, if the center-to-center distance between nearest neighbors is 4 nm (e.g., $R = 1.5$ nm, $D = 1$ nm), the center-to-center distance for particles in the sixth coordination sphere will be 9.8 nm, well within the validity range for eq 1. For superlattices of large (>10 nm) nanocrystals, retardation must be taken into account. Our analysis shows that the retardation effect will decrease γ_t in superlattices of large nanocrystals, making the trend shown in Figure 4c even stronger (Figure S4).

The data in Figure 4c revealed another important trend: γ_t decreases with increasing interparticle spacing. This means that superlattices of nanocrystals with short ligands (e.g., butylamine, tributylphosphine, etc.) should be less susceptible to formation of twin planes than those with longer ligands (e.g., oleylamine, oleic acid, etc.). Indeed, this prediction agrees with experimental observations: superlattices of CdSe nanocrystals capped with TOPO/TOP ($D \approx 1$ nm) rarely show MT-SLs and are generally less twinned than superlattices of oleic acid-capped PbS nanocrystals ($D \approx 1.4$ nm).

Why Does the Formation of Multitwinned Superlattices Depend on the Nanocrystal Size? The size dependence of γ_t explains why superlattices composed of larger nanocrystals are much more susceptible to formation of twin planes: introducing a twin plane costs significantly more energy in superlattices of small nanocrystals compared to larger nanocrystals. At the same time, understanding the size-dependent appearance of MT-SLs requires a more rigorous analysis of relative energies for twinned and nontwinned superlattice structures based on the comparison of γ_t to other characteristic parameters of the superlattice. Multiple twinning has been extensively studied in atomic systems. Ino[20,27] and Marks[21,29,30] used a modified Wulff construction to minimize crystal surface energy. Marks introduced the dimensionless parameter ε_ω, which describes the total surface energy of a fcc crystal with twin planes and is dependent only on the crystal shape and not on the volume.[30] Marks has shown that thermodynamically stable decahedral crystals should deviate from a perfect decahedron and form re-entrant 111 surfaces at the twin boundaries, leading to a shape known as Marks's decahedron (M-Dh).[30] We routinely observed such re-entrant planes in MT-SLs with both decahedral and icosahedral geometries (Figures 1 and 2). Through minimization of the surface energy, Marks derived the following expressions for ε_ω for nontwinned fcc crystals (SC) and multiply twinned crystals with decahedral (M-Dh) and icosahedral (Ic) symmetry, respectively:[30]

$$\varepsilon_\omega^{\mathrm{SC}} = \{108\sqrt{3}(1 - 3\beta^3)\}^{1/3} \quad (2)$$

$$\varepsilon_\omega^{\mathrm{M-Dh}} = \{101.25\sqrt{3}[(1 + \eta)^3 - {}^8/_3(\beta^3 + \eta^3)]\}^{1/3} \quad (3)$$

$$\varepsilon_\omega^{\mathrm{Ic}} = \{67.5\sqrt{3}[(1 + 3\eta)^3 - 24\eta^3]\}^{1/3} \quad (4)$$

where the relative surface energies of SC, M-Dh, and Ic crystals are expressed in terms of the two dimensionless parameters $\eta = \gamma_t/(2\gamma_{111})$ and $\beta = 1 - \gamma_{100}/(\sqrt{3}\gamma_{111})$,which relate the twinning energy and the energy of the 100 surface facet (γ_{100}) to the energy of the 111 surface facet (γ_{111}).

Like any solid, a nanocrystal superlattice has a surface energy associated with the different coordination of nanocrystals in the bulk of the superlattice compared to those on the surface, where many interparticle "bonds" are broken. The surface energy of a particular facet (γ_{hkl}) can be calculated as half the energy needed to break the interparticle bonds per unit area:

$$\gamma_{111} = 2\sqrt{3}(\phi_1 + \phi_2 + 4\phi_3)/a^2 \quad (5)$$

$$\gamma_{100} = 2(2\phi_1 + \phi_2 + 8\phi_3)/a^2 \quad (6)$$

$$\gamma_{110} = 2(3\phi_1 + 2\phi_2 + 10\phi_3)/a^2 \quad (7)$$

where ϕ_1, ϕ_2, and ϕ_3 are the pairwise interaction energies between first, second, and third near neighbors in the superlattice, respectively.

As discussed above, ϕ_2 and ϕ_3 can be described by the van der Waals interactions between the inorganic cores ($U_{\mathrm{vdW}}^{\mathrm{PbS-PbS}}$). However, the expression for ϕ_1 is much more complex and includes direct ligand−ligand interactions ($U^{\mathrm{L-L}}$). According to recent studies, short-range vdW interactions between interdigitated hydrocarbon ligand molecules can be very strong. In vacuum, the attraction between hydrocarbon ligands can be more than an order of magnitude stronger than the attraction between inorganic components.[49,51,52] However, in the presence of a good solvent, ligand−ligand interactions become strongly repulsive due to steric and osmotic forces, thus imparting colloidal stability on nanocrystal dispersions in toluene and other nonpolar solvents.[49] To the first order, both attractive and repulsive interactions between ligand molecules should be proportional to the overlap volume (V_L) between the ligand shells of two nanocrystals capped with ligand molecules of effective length L (Figure 4a). Therefore, ϕ_1 can be approximated as

$$\varphi_1 = U^{\mathrm{PbS-PbS}} + U^{\mathrm{L-L}} \approx U_{\mathrm{vdW}}^{\mathrm{PbS-PbS}} + \xi(L, D)V_L \quad (8)$$

where $\xi(L,D)$ describes ligand−ligand interactions per unit overlap volume and can include various forces, while

$$V_L = \frac{\pi}{2}(2L - D)^2R + \frac{\pi}{6}(2L - D)^2(2L + D/2) \quad (9)$$

The last expression, V_L, provides an estimate for scaling the magnitude of the ligand−ligand interactions with nanocrystal size as a function of the overlap. The dependence of γ_{111} on nanocrystal size was calculated for the limiting cases of $|U^{\mathrm{PbS-PbS}}| \gg |U^{\mathrm{L-L}}|$ and $|U^{\mathrm{PbS-PbS}}| \ll |U^{\mathrm{L-L}}|$, shown in Figure 5a and b, respectively. Similar dependences for γ_{100} and γ_{110} are shown in Figure S5. One can see that, in the limit of $|U^{\mathrm{PbS-PbS}}| \gg |U^{\mathrm{L-L}}|$ (strong interaction between inorganic components), γ_{111} strongly depends on the interparticle separation and generally increases with increasing nanocrystal size for $D > 0.5$ nm. With known γ_t, γ_{111}, and γ_{100}, we calculated η and β parameters in the Marks model (Figures S6 and S7) and found that both η and β strongly decrease with increasing nanocrystal size. Generally, small η and β favor thermodynamic stability of multitwinned structures, and the calculated trend is in agreement with the experimentally observed transition from nontwinned to twinned nanocrystal superlattices with increasing nanocrystal size (Figures 1 and 2).

If ligand−ligand interactions dominate over the vdW forces between inorganic cores ($|U^{\mathrm{PbS-PbS}}| \ll |U^{\mathrm{L-L}}|$), the surface energy of the fcc superlattice decreases with increasing nanocrystal size as $\sim R^{-1}$ (Figure 5b). In this limiting case, the parameter η shows a weak size dependence (Figure S8), while $\beta = 1/3$ is size-

(51) Landman, U.; Luedtke, W. D. *Faraday Discuss.* **2003**, *125*, 1–22.
(52) Mueggenburg, K. E.; Lin, X. M.; Goldsmith, R. H.; Jaeger, H. M. *Nat. Mater.* **2007**, *6*, 656–660.

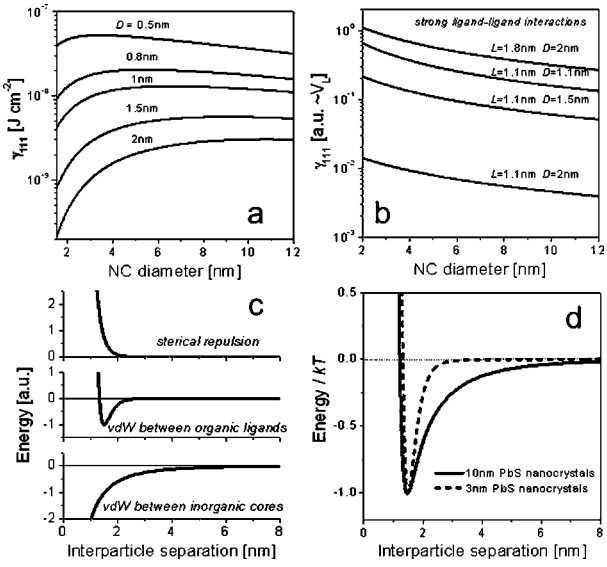

Figure 5. (a) Surface energy of the 111 facet of fcc nanocrystal superlattice vs nanocrystal diameter for different interparticle gaps (D) calculated for the case of strong van der Waals interactions between inorganic cores. (b) Surface energy of the 111 facet of fcc nanocrystal superlattice vs nanocrystal diameter for different effective lengths of ligand molecules (L) and D calculated for the case of strong interactions between the organic ligands. (c) Scaling behavior for different terms contributing to the interparticle pair potentials. (d) Pair potentials for two PbS nanocrystals during self-assembly of the nanocrystal superlattice. Large (10 nm) PbS nanocrystals exhibit softer potentials compared to small (3 nm) nanocrystals. See text for details.

independent. Taking into account that U^{L-L} can have very different values depending on the solvent polarity, we need additional information about the absolute magnitude of ϕ_1 in order to know which of these two regimes occurs *during* the self-assembly of nanocrystals into a superlattice.

In our experiments, the slow diffusion of ethanol into toluene (Figure 1c) resulted in a gradual increase in solvent polarity and a switch from repulsive to attractive ligand−ligand interactions. Nanocrystal superlattices nucleated and grew when the interparticle potentials became appropriate for the formation of a long-range ordered structure. High-resolution SEM studies confirmed layer-by-layer growth of the superlattice, where the nucleation of a new layer of nanocrystals occurred only after substantial completion of the underlying layer (Figure S9). This growth mechanism puts certain requirements on the strength of the interparticle interactions. Layer-by-layer growth of the 111 facet of a fcc crystal requires that an incoming nanocrystal should sample multiple surface sites before landing on the most favorable one. In the simplest form, this implies that a nanocrystal should be weakly bound to the surface when it has only three nearest neighbors, whereas nine nearest neighbor bonds should solidly hold it in place. The growth of a layer occurs by adding nanocrystals to the edge of the growing layer with five or six nearest neighbors at step edges and kinks, respectively (Figure S10). Such growth conditions can be satisfied when $0.5 < \phi_1/k_BT < 1.2$ (k_B is the Boltzmann constant and T is the temperature) during the self-assembly process. This conclusion can also be tested by directly counting the concentration of missing nanocrystals in 111 facets of PbS superlattices and using the Boltzmann factors to estimate the interaction energy of a nanocrystal with its nearest neighbors. The Boltzmann factor, $\exp(E_i/k_BT)$, determines the relative probability of state i with energy E_i in a multi-state system in thermodynamic equilibrium at temperature T. The ratio of the probabilities of two states is given by the ratio of their Boltzmann factors. From HRSEM images of superlattices, we measured the concentration of empty sites in 111 facets, corresponding to the probability for a nanocrystal to leave the nine-coordinated site ($E = 9\phi_1$), forming a state with $E = 0$. Then, assuming that the self-assembly of PbS nanocrystal superlattices is a not-far-from-equilibrium process, which makes sense taking into account its structural perfection, we found the density of empty sites in the 111 superlattice facet to be between 10^{-4} and 10^{-3}, corresponding to $0.77 < \phi_1/k_BT < 1$ for superlattices of 10 nm PbS nanocrystals.

Knowing an approximate value of ϕ_1, we can compare the contributions of $U_{vdW}^{PbS-PbS}$ and U^{L-L} to the interparticle potential for different nanocrystal sizes. For two 3 nm PbS nanocrystals separated by a 1.5 nm layer of hydrocarbon ligands, $U_{vdW}^{PbS-PbS} \approx 1$ meV $\ll k_BT$, implying that interactions between inorganic components cannot be sufficient to induce self-assembly of nanocrystals, and $U^{L-L} \gg U_{vdW}^{PbS-PbS}$. In contrast, in the case of 10 nm PbS nanocrystals with $D =$ 1.5 nm, $U_{vdW}^{PbS-PbS} \approx 25$ meV $\approx k_BT$, and we can conclude that $U_{vdW}^{PbS-PbS} > U^{L-L}$, opposite to the 3 nm case! According to our analysis, the dominant force for the assembly of nanocrystals into a superlattice is ligand−ligand interactions for small (3 nm) PbS nanocrystals and inorganic core−core interactions for large (10 nm) PbS nanocrystals. We used eq 1 and the Lennard-Jones potential to model $U_{vdW}^{PbS-PbS}$ and U^{L-L}, respectively (Figure 5c). Steric repulsion was described as proposed by Korgel et al.[4] Figure 5d compares the interparticle potentials for two 3 nm and two 10 nm PbS nanocrystals. Rather counterintuitively, 3 nm PbS nanocrystals, whose potential is dominated by U^{L-L}, exhibit a very sharp minimum, corresponding to "hard" particle−particle interactions. At the same time, 10 nm PbS nanocrystals show "softer" potentials, with interparticle interactions dominated by $U_{vdW}^{PbS-PbS}$.

The difference in the interactions between small and large nanocrystals is in line with the observed size-dependent twinning behavior. The "decision" to form either a perfect fcc lattice or a multiply twinned one is made during the nucleation event, when a small number of nanocrystals arrange themselves into a cluster with corresponding geometry. An alternative approach to study twinning is based on the direct modeling of the structure of clusters formed during the early stage of crystal formation.[53] It was found that the lowest energy cluster structure depends on the pair potentials and on the number of assembling particles.[53,54] According to Doye, Wales, and Berry, "soft" interatomic potentials favor multitwinned Ic and M-Dh structures, whereas "hard" potentials lead to fcc crystals.[55] This behavior results from the ability of clusters with "soft" potentials to more easily release the elastic strain inherent in multi-twinned lattices (see next section).[53,55] We want to emphasize that these potentials act during the assembly of the superlattice, whereas removal of solvent can significantly change the relative contributions of $U_{vdW}^{PbS-PbS}$ and U^{L-L}, most probably by strengthening the latter component.

How Does Strain Relax in Multiply Twinned Nanocrystal Superlattices? In general, the stability of MT particles is determined by the interplay of three factors: (i) the surface energy decreasing as a result of increased exposure of low-

(53) Baletto, F.; Ferrando, R. *Rev. Mod. Phys.* **2005**, *77*, 371–423.
(54) Bytheway, I.; Kepert, D. L. *J. Math. Chem.* **1992**, *9*, 161–180.
(55) Doye, J. P. K.; Wales, D. J.; Berry, R. S. *J. Chem. Phys.* **1995**, *103*, 4234–4249.

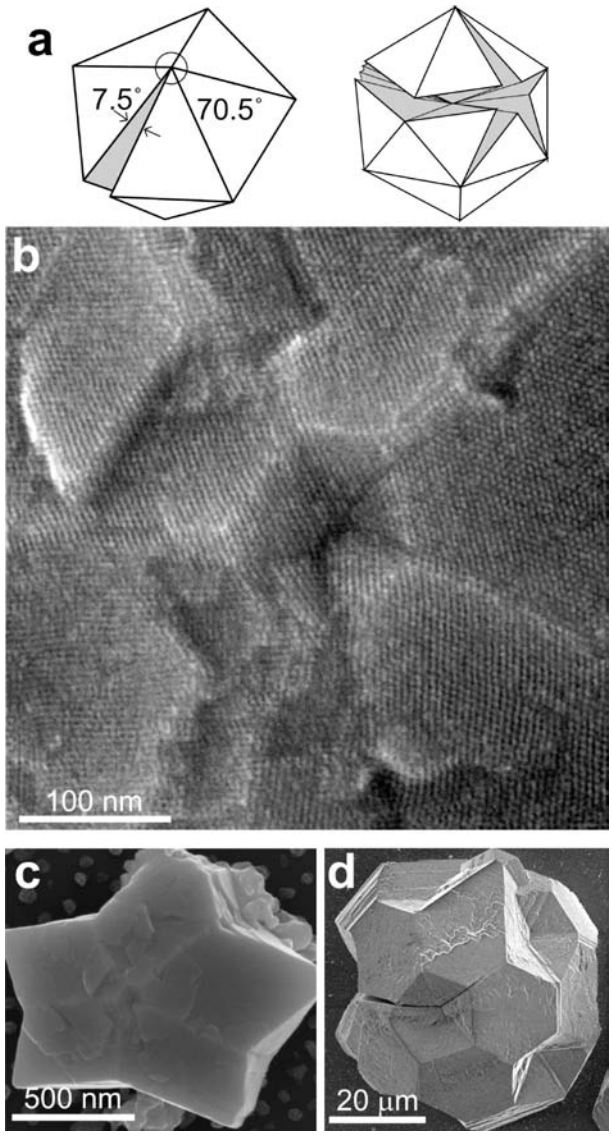

Figure 6. (a) Solid angle deficiency in multiply twinned nanocrystal superlattices leads to elastic strain proportional to volume of the superlattice. (b) High-resolution SEM image taken along the five-fold axis of the multiply twinned superlattice shown in panel (c). (d) Removal of the occluded solvent molecules increases the shear modulus of the superlattice, which can relax by opening a gap as shown in panel (a).

energy 111 facets, (ii) the twinning energy needed to form the twinning planes, and (iii) the elastic energy necessary to accommodate the strain inherent to MT structures. This strain originates from the solid angle deficiency in MT structures (Figure 6a). In a nonstrained fcc lattice, five twin planes should be rotated by 70.5° about a common axis; however, this results in a lattice mismatch of 7.5° (Figure 6a), which must be accommodated in the structure. To fill the space without gaps, the interparticle distances should deviate slightly from the ideal distances for a fcc lattice, leading to the strain energy contributing to the free energy of M-Dh and Ic superlattices. Since strain energy is proportional to the crystal volume, its contribution is relatively small in small crystals, while it becomes dominant as crystal size increases.[29] At a certain size, the MT structure becomes metastable with respect to a perfect crystal. As a result, eqs 2−4 can be applied only to very small crystals.[30] In many atomic crystals, the lowest energy structure switches from Ic, which is the most strained but has the lowest surface energy, to M-Dh and, finally, to SC as the crystal size increases.[53] Atomic clusters can undergo these phase transitions upon heating, but transitions in nanocrystal superlattices would be very improbable at room temperature, and the MT phase should continue growing in the metastable regime.[29,56] MT-SL can either incorporate elastic stress via expansion/contraction of the interparticle distances or relax strain by incorporating structural defects.[32,33,42,57,58]

MT-SLs provide a convenient route to study different relaxation pathways in multitwinned crystals, as they offer the possibility to look at the structure in real space with single-particle resolution (Figure 6b,c). We found that there is no single way of dealing with strain in PbS MT-SLs. In many cases, the superlattices accumulated elastic energy without introducing any structural defects. The presence of residual solvent molecules occluded by the superlattice "softens" the interparticle potentials, helping to accommodate the elastic strain. After the crystals are removed from the solvent, these residual solvent molecules slowly evaporate. In this case, the ligand−ligand interactions become stronger, increasing the shear modulus of the superlattice. In some cases, drying of the superlattices resulted in crack formation around the five-fold axis (Figure 6d). This observation provides additional evidence that the interparticle forces acting during assembly of a superlattice differ substantially from those acting after solvent evaporation. In addition to strain release via opening of a gap (Figure 6d), some MT-SLs relaxed the elastic strain by introducing disclinations (Figures S11−S13).

4. Conclusions and Outlook

The experimentally observed dramatic increase of the twinning probability with increasing nanocrystal size is likely a result of both the size dependence of the twinning energy, shown in Figure 4c, and the "softer" interparticle potentials active during assembly of larger nanocrystals. Twinning in atomic clusters and crystals has been a subject of intense study during the past few decades. The possibility to manipulate the interparticle potentials combined with direct imaging of the superlattice surface with single-particle resolution provides additional degrees of freedom, which were lacking in previously studied atomic systems. The presence of twin planes in nanocrystal superlattices also has implications in the fabrication of nanocrystal-based devices, such as photodetectors and solar cells. At the same time, twin planes should not strongly impact transport properties, since the immediate environment of the nanocrystal is unperturbed.

Acknowledgment. We thank M. Kovalenko, T. Witten, E. Wong, and B. Spokoyny (University of Chicago) for stimulating discussions. D.V.T. acknowledges support from the NSF MRSEC Program under Award No. DMR-0213745 and NSF CAREER under Award No. DMR-0847535. The work at the Center for Nanoscale Materials (ANL) was supported by the U.S. Department of Energy under Contract DE-AC02-06CH11357.

(56) Barnard, A. S.; Young, N. P.; Kirkland, A. I.; van Huis, M. A.; Xu, H. F. *ACS Nano* **2009**, *3*, 1431–1436.
(57) Barnard, A. S. *J. Phys. Chem. B* **2006**, *110*, 24498–24504.
(58) Johnson, C. L.; Snoeck, E.; Ezcurdia, M.; Rodriguez-Gonzalez, B.; Pastoriza-Santos, I.; Liz-Marzan, L. M.; Hytch, M. J. *Nat. Mater.* **2008**, *7*, 120–124.

Supporting Information Available: Figure S1, models and experimentally observed crystals; Figure S2, scheme showing the nearest neighbors around twin plane; Table S1, number and distances of nearest neighbors; Figure S3, electrophoretic mobility data for PbS nanocrystals in toluene; Figures S4−S8, additional energetic contributions and considerations; Figures S9, SEM image and Figure S10, scheme illustrating layer-by-layer growth of superlattices; and Figures S11−S13, SEM images of strain relaxation in PbS superlattices. This material is available free of charge via the Internet at http://pubs.acs.org.

JA9074425